WATER RESOURCES RESEARCH, VOL. 21, NO. 3, PAGES 281–296, MARCH 1985

Exploration of a Rigid Ice Model of Frost Heave

KEVIN O'NEILL

U.S. Army Cold Regions Research and Engineering Laboratory, Hanover, New Hampshire

ROBERT D. MILLER

Cornell University, Ithaca, New York

A numerical model is explored which simulates frost heave in saturated, granular, air-free, solute-free soil. It is based on equations developed from fundamental thermomechanical considerations and previous laboratory investigations. Although adequate data are lacking for strict experimental verification of the model, we note that simulations produce an overall course of events together with significant specific features which are familiar from laboratory experience. Simulated heave histories show proper sensitivities in the shapes and orders of magnitude of output responses and in the relations between crucial factors such as heave rate, freezing rate, and overburden.

INTRODUCTION

The phenomenon of frost heave includes processes whereby soil freezing induces a moisture flow, beyond that caused by the mere expansion of water on freezing. In our common experience, heave is identified with the upward displacement of the soil surface, forced by transport processes below the surface as freezing occurs. The amount of heave is equal to the amount of that displacement. This phenomenon may occur cyclically due to environmental influences, may proceed monotonically for periods on the order of the lifespan of a structure, or may even progress indefinitely. Every year, frost heave damages or destroys public and private property worth billions of dollars, even as additional billions are being invested in measures intended to prevent or mitigate future damage. To be cost effective, such measures must be based on realistic estimates of the heaving behavior of the soil, known to be strongly dependent on soil characteristics as well as environmental variables. Coarse sands and gravels are not susceptible to heave. Silts can produce spectacular heave, but only if the load to be heaved is small and the water table is high. Clays never produce spectacular heave, but can still merit serious consideration due to their ability to heave very large loads indeed. Clearly, a system for evaluating the tendency to heave must take into account the causal physics, which is reflected in this varied picture of conditions and consequences.

One mode of heave, called primary heave, consists of a layer of ice growing on top of some unfrozen soil, through which liquid water is drawn to join the ice. This system may or may not be overlain by frozen soil. In either case, essentially no ice penetrates the remaining unfrozen soil, and all freezing contributes directly to the surface heave. Alternatively, in what has been called the secondary mode of heave, ice penetrates the soil; at the same time, the liquid flow towards the ice feeds an accumulation of ice within the frozen soil. Lenses of pure, segregated ice grow within forced discontinuities in the frozen soil fabric. This in turn forces movement, sometimes quite powerful movement, of the soil surface. At the opposite extreme from primary heave, soil freezing may result in no heave at all when all ice formed penetrates the soil. Between these two limiting possibilities lies the secondary mode. Depending upon the properties of a soil and boundary conditions of the narrow zone in which freezing is actually taking place, any of these three possibilities may result when soil freezes or, over time, all three may be traversed. It is the secondary mode in which greatest loads are lifted, which is of greatest engineering interest, and which is the main focus of this paper.

Relevant boundary conditions include the magnitude of the load to be heaved, and this includes the weight of soil that is already fully frozen. They include the rate at which heat is being extracted through the cold boundary of the frozen zone as well as the rate at which heat is being absorbed from as yet unfrozen soil. Another important boundary condition is the water pressure at the warm boundary which, in turn, is influenced by hydrologic conditions at greater depths. If no heave is taking place, water will be expelled from a descending zone of freezing into unfrozen soil due to the expansion of water on freezing. During primary heave, by contrast, water is absorbed from the unfrozen zone to the freezing site at the same (mass) rate that segregated ice forms. In secondary heave, flow may be in either direction and the direction may reverse with time. All of these processes interact in ways too devious to permit intuition or simplistic idealizations to tell us what to expect over periods of time ranging from as little as a few hours to as long as tens of years.

For engineering purposes, a large number of lab tests, prescriptions, rules of thumb, and methods for characterizing soils and situations has been developed over the years in an attempt to provide practical guidance on the likelihood of heave and its magnitude [*Chamberlain*, 1981]. The sheer number and variety of these approaches and procedures is forceful testimony to the difficulty of the problem, to the absence of any common understanding of it, and to the inadequacy of any established approach for general application. In response, researchers have developed increasingly sophisticated mathematical models, attempting to reduce uncertainty by including superior representations of relevant physics and thermodynamics. The overall offerings in this domain and many of the underlying concepts are reviewed by *O'Neill* [1983]. For further discussion of some of the basic concepts and equations adduced below, the reader is referred to this review and to the textbook treatment by *Miller* [1980].

Among responses to the challenge is what has been called

Paper number 4W1404.
0043-1397/85/004W-1404$05.00

the rigid ice model of frost heave. This model is comprised of a set of macroscopic equations which result from an analysis of the microscopic features of the formation of ice from water within the pores of a soil [*Miller*, 1978]. At present, the physical formulation is limited to solute-free, air-free soils of negligible compressibility. A simplified set of equations applicable only to very simple quasi steady states has been solved by *Miller and Koslow* [1980]. A strategy for obtaining numerical solutions of the full set of equations for simple boundary conditions has also been developed [*O'Neill and Miller*, 1982]. In this paper we expand on the physical basis of that formulation and its mathematical expression and implementation. Improved tactics have produced a more flexible model so that its behavior can be better explored. We report examples of the results of such explorations below.

PHASE EQUILIBRIA

Concepts of phase equilibrium applicable at a microscopic level are most familiar in the context of water and air in (ice-free) porous media. It is useful to paraphrase these to establish a rationale for the treatment of ice-water equlibria in air-free soil. The adjective microscopic, as used in this paper, refers to scales that are large relative to the dimensions of a single molecule or the length of chemical bonds but small compared to the scale of observation. Relevant scales are those comparable to the dimension of grains, interstices between them, and even "long-range" surface adsorption force fields. A well-known example of the last is the virtual force field that arises if there is a diffuse electrical double layer at a grain surface. In this discussion, no particular model of surface adsorption will be invoked. Instead, we merely use a more general proposition that for whatever reasons, liquid water very close to a grain surface is attracted toward that surface and that the attractive force is greater for liquid than for air or ice, other things being equal. The strength of this attraction decays with distance from the surface.

This implies that a grain immersed in water will be surrounded by a microscopic "hydrostatic" pressure field. We then perceive that to the extent that some other less strongly attracted substance displaces water from this field, that substance will appear to be repelled by the grain by a disjoining force. This force is an analogue of what we call the buoyant force on a body that displaces water from within a hydrostatic field induced by gravitation.

If a bubble of air approaches an immersed grain, it will experience a disjoining force which can be balanced by increasing the air pressure in that part of the bubble which is outside the force field and where both water and air pressures can ostensibly be controlled or measured. Disregarding surface tension effects, the degree to which air can displace water from what we would now call an adsorbed film of mobile water depends upon the difference, ϕ_{wa}, between water and air pressure outside the effective range of the adsorption force. That same measured difference determines the mean curvature of the water-air interface outside the force field and hence the degree to which air replaces water in capillary space. Therefore within a rigid pore system the degree to which air displaces water from adsorbed films on the one hand and from capillary space on the other hand is a function of the quantity ϕ_{wa} defined as $u_w - u_a$. The symbols u_w and u_a represent gauge pressures in liquid water and air, respectively, with respect to a standard atmosphere. Thus in a unit macroscopic volume of unfrozen soil the volumes W of unfrozen water and F of air and G of grains are complementary functions of ϕ_{wa}

$$W(\phi_{wa}) + F(\phi_{wa}) + G = 1 \tag{1}$$

In this equation and in what follows we proceed in terms of macroscopic variables, i.e., in quantities measurable at the scale of actual observations, equal to mean or average values of their microscopic counterparts.

If, at temperatures not too far below 0°C the specific surface energies of crystal-melt interfaces of ice are independent of crystallographic orientation, exactly the same mechanical concepts enter into the displacement by ice of water from adsorption space on the one hand and capillary space on the other hand, and we write for air-free soil

$$W(\phi_{iw}) + I(\phi_{iw}) + G = 1 \tag{2}$$

where

$$\phi_{iw} \equiv u_i - u_w \tag{3}$$

and where u_i is ice pressure relative to standard atmospheric pressure, again as measured in capillary space, and I is volumetric ice content. Because u_w has been defined as gauge pressures with respect to standard atmospheric pressure, we find that integration of an appropriate form of the Clausius-Clapeyron equation yields

$$u_w - (\rho_w/\rho_i)u_i = (\rho_w L/273)T \tag{4}$$

where T is the equilibrium temperature in degrees Celsius, ρ is the density of the indicated phase, and L is the latent heat of fusion of water per unit mass. If the ratio (ρ_i/ρ_w) is defined as γ_i, the specific gravity of ice, and if $(\rho_w L)$ is denoted as H, the heat of fusion of a unit volume of liquid water, then

$$u_w - u_i/\gamma_i = (H/273)T \tag{5}$$

Elimination of u_i between (3) and (5) yields

$$\phi_{iw} = (\gamma_i - 1)u_w - (\gamma_i H/273)T \tag{6}$$

Thus in a rigid porous medium, in the absence of air, unfrozen water content and ice content are complementary (hysteretic) functions of ϕ_{iw} only, and we conclude that ϕ_{iw} is a function of temperature and water pressure. We note further that at least within a certain range, ice content is a continuous (hysteretic) function of those variables. All soil water does not freeze at any given temperature, a fact underscored in various experimental studies [e.g., *Koopmans and Miller*, 1966; *Tice et al.*, 1978; *Horiguchi and Miller*, 1983].

For a soil in which the volume of capillary space is very large relative to the volume of adsorption space, the functions I and W in air-free soil and W and F in ice-free soil are scarcely affected by the influence of ϕ_{iw} and ϕ_{wa}, respectively, on film thickness. However, these functions are strongly related to the influence of ϕ_{wa} and ϕ_{iw} on the mean curvature of the interfaces in capillary space. In particular, when matching values of W are achieved by freezing of air-free soil on the one hand, or by drying of ice-free soil on the other hand $(W(\phi_{wa}) = W(\phi_{iw}))$, interfacial curvatures should match. In this condition the mean phase interface curvature $(1/r_{wa})$ in a volume of ice-free soil equals $(1/r_{iw})$ for air-free frozen soil or

$$\phi_{wa} = (\omega_{wa}/\omega_{iw})\phi_{iw} \tag{7}$$

where ω designates the surface tension. This proposition was tested [*Koopmans and Miller*, 1966], and a value 2.20 was indicated for the ratio $\omega_{wa}(20°C)/\omega_{iw}$. This value agrees reasonably well with evaluation by other means and hence supports the application of capillary concepts in freezing of noncolloidal soils.

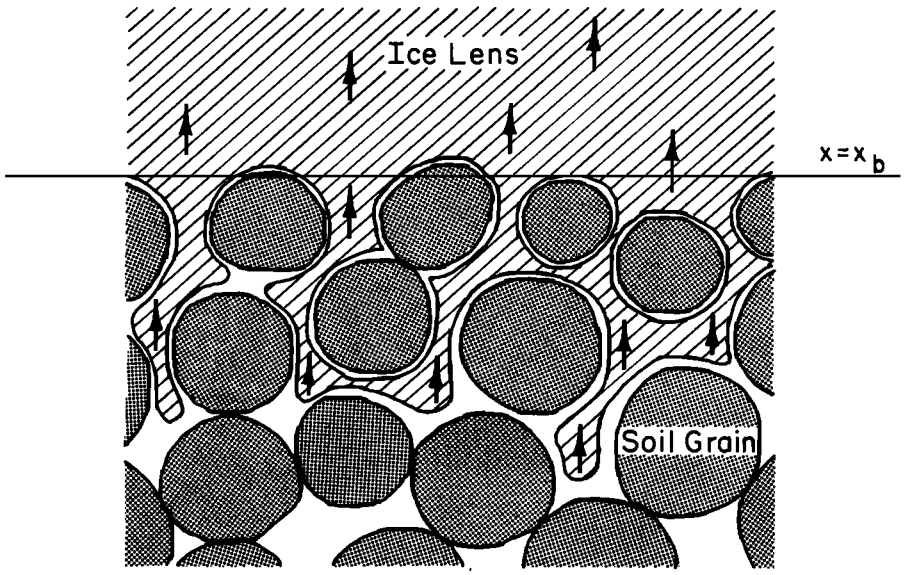

Fig. 1. Schematic diagram of the frozen fringe, with ice lens above.

At the other extreme is the case in which the volume of capillary space is trivial or nonexistent relative to the volume of adsorption space, as in a paste of a highly colloidal clay mineral. If, when held at equal distances from grain surfaces by mobile films of adsorbed water, equal volumes of ice and [illegible] would also experience the same disjoining force and ϕ_{iw} and ϕ_{wa} would be numerically equal. Thus $W(\phi_{iw})$ for air-free soil and $W(\phi_{wa})$ for ice-free soil should match. It seems likely that the adsorption forces for ice and water would be perceived as equal only if both were trivial or zero; both would be zero for the double layer model, for example. *Koopmans and Miller* [1966] used Na montmorillonite to test and confirm postulated equalities of $W(\phi_{iw})$ and $W(\phi_{wa})$ for numerically equal values of ϕ_{iw} and ϕ_{wa} in highly colloidal systems.

We dwell on this matter because a number of papers in the last decade or so have been based on the explicit or implicit assumption that one can always use the functions $W(\phi_{wa})$ and $F(\phi_{wa})$ obtained above freezing for $W(\phi_{iw})$ and $I(\phi_{iw})$, respectively, applied below freezing. This would be valid in a highly colloidal soil but not in a soil low in colloids. The situation is even more complex when both ice and air are present. However, in this paper attention is confined to air-free incompressible soils, i.e., soils in which colloids, if present, have negligible influence. Other common pitfalls in the relations used between phase pressures and phase composition are discussed by *O'Neill* [1983].

Thermally Induced Regelation and the Basic Scenario

The rationale for the rigid ice model is based on a corollary of a deduction, confirmed by experiment, concerning the behavior of isolated grains embedded in ice. It follows from the proposition that liquid water is attracted by grain surface more strongly than is rigid crystalline ice. If that is true, then at temperatures somewhat below 0°C the grain ought to be surrounded by a film of unfrozen liquid in equilibrium with the ice. If a temperature gradient is imposed, thermal equilibrium of water and ice at the interface is inconsistent with mechanical equilibrium in the hydrostatic field induced by surface adsorption forces. Whereas the thermal gradient induces asymmetry of film thickness, the action of adsorption forces is to center the grain within its liquid shell. Thus the temperature field constantly acts to diminish the film thickness on the cold side, while surface forces seek to retain that film thickness by removing ice from the warm side and transporting the resulting unfrozen water to the cold side, where it refreezes. The grain ought to migrate up the temperature [illegible] ever warmer environment with a corresponding increase in average thickness of the film, expediting the flow of liquid by which the centering tendency is expressed. This deduction was apparently confirmed by a single pair of photographs [*Hoekstra and Miller*, 1965], leading to construction of special apparatus which allowed many individual grains to be tracked and their velocities measured [*Römkens and Miller*, 1973].

If individual grains migrate through stationary rigid ice, traveling up a temperature gradient, then rigid ice that largely fills interstices between stationary grains ought to migrate down a temperature gradient. If the ice is inherently rigid, this movement is not flow but continuous regelation. Crystalline ice, everywhere bounded by liquid in both adsorption and capillary space, is continuously melting and reforming in a manner consistent with the geometry imposed by the array of soil grains. As many experimentalists have learned from experience, wet soil is easily supercooled by as much as several degrees in the absence of effective nucleation sites. It is customary to minimize this by seeding crystallization or inducing nucleation by mechanical or thermal shock. This means that once freezing begins, essentially all ice formed thereafter will grow sequentially through the pore system, forming on preexisting ice. This generates one geometrically complex but nevertheless solidly interconnected ice body. Thus as the ice migrates through the grains by regelation, it moves as a solid body at a spatially uniform velocity. This is diagrammed, albeit crudely, in Figure 1, which includes moving pore and lens ice. Temperature increases from the bottom of the figure, through the freezing front where soil ice first appears and into the lens above. The lens occupies a discontinuity in the soil fabric, while within the whole soil the pore ice content varies continuously according to conditions, as outlined above. On the warm side of the lens, x_b designates the macroscopic position of the lens–frozen soil interface. This corresponds microscopically to a wiggley surface separating the lens ice from soil grains and pore ice below. The partially frozen zone between

the warm side of the lens and the freezing front is designated as the "frozen fringe."

This vision of the mechanism of frost heave must be thought about with some care. For example, consider that the thermal field is stationary, and ice is moving as diagrammed in Figure 1, while the soil grains remain stationary. Then the water flux in the ice-free zone must be equivalent to the ice flux represented by movement of the ice lens, corrected for the lower density of ice. If the ice were immobile (not shown) but the thermal field descending, ice content would be increasing with time at every level, with a corresponding expulsion of water through the ice-free zone. If the ice is moving upward at the same time that the thermal field is descending, the velocity of water just below the ice lens will generally be upward. However, if the upward ice velocity is slow enough, relative to the rate of descent of the thermal field, water velocity may be zero at some level between the ice lens and the freezing front and will be downwards below that level. This is discussed further in the context of the simulations.

In the ice lens, only ice is present to support what lies above, including any applied surcharge. Ice pressure in the lens is fixed by that total load, hereafter called the overburden P. In ice-free soil below the load supported by stressing of grain contacts includes not only the overburden but the virtual load that will arise if the pressure of pore water in capillary spaces is less than atmospheric. In the frozen fringe zone the overburden must be balanced, augmented by any virtual load due to negative water pressure plus the effects of ice-water surface tension. However, this will be offset in some degree by the pore ice, if its pressure is greater than atmospheric pressure. While ice pressure will be somewhat less than film pressure at a convex film, its pressure will exceed that of water in capillary spaces by an amount given by the Clausius-Clapeyron equation. Thus if ice pressure and ice content are high enough at some point in the frozen fringe so that ice forces balance the combined overburden plus virtual pore water load, then nothing is left to stress grain contacts. Grains above that level can be carried along en masse by moving ice, which is always moving upward (down the thermal gradient), and we will perceive the initiation of new ice lens. It makes sense mechanically that as freezing progresses through the soil, new lenses should form somewhere within the frozen zone. It this were not so it would imply that the greatest load bearing by and ultimate concentration of ice would develop at the leading edge of the frozen zone (the freezing front), where ice concentration and ice pressure are least. Experiments have confirmed the appearance and ensuing growth of ice lenses behind the freezing front in both near-colloidal [e.g., *Hoekstra*, 1969] and noncolloidal soil [e.g., *Loch and Kay*, 1978]. To know when this will happen we need to know where and when intergranular stresses reach zero. It turns out that this is always at a finite distance below the base of an existing ice lens.

In thinking about this we recognize that for a given thermal gradient, one might expect ice to move rapidly near the freezing front and more slowly near the ice lens. However, if it is rigid, its velocity (but not its flux) must be uniform. Ice flux is simply the product of this velocity and the ice content, which is unity in an ice lens. Thus the ice velocity is identical to "rate of heave."

A number of frost heave models which contrast in general with the one presented here do, however, share the feature that segregated ice is assumed to form within the frozen soil. In some cases an attempt is also made to use some of the concepts advanced in the paragraphs above to characterize a frozen fringe and the transport through it. However, no other model considers the ice within the fringe to be mobile, except perhaps by indirect implication. More specifically, none assumes pore ice motion by regelation. The two models closest to ours are those by *Hopke* [1980] and *Gilpin* [1980], each of which entails transport through the fringe in some central way. Hopke's simulated results are qualitatively appealing, but he reports limitations on the tractability of the calculations. These might be due to use in three phase situations (ice, water, air) of $W(\phi_{wa})$ relations suitable only for two phase freezing (ice, water). Gilpin indicates that he set out to simplify for simulation purposes the system proposed by *Miller* [1978]. His idealization which probably constitutes the greatest physical departure from our perspective is his assumption that all freezing takes place at the base of the warmest lens, or at the leading edge of the frozen fringe. Both of these models assume that all segregation freezing occurs at the base of a growing lens and neither allows heave (ice motion) within the fringe.

While we find it difficult to construct a credible heave scenario without the assumption of rigid ice undergoing regelation, it must be acknowledged that no incontravertible experimental validation of the proposition exists, and therefore it must still be introduced as an assumption. It is instructive to consider the alternative assumptions one could bring to bear to explain away the difficulties posed by the obvious connection between moving lens ice and ice in the fringe. Even in other heave models in which fringe ice is immobile, one or another alternative must be implied at least at the lens-fringe connection. One can assume either (1) that lens ice is, in fact, not solidly connected to pore ice in the fringe, that is, that microscopic connections break as necessary sometime after the lens has formed; or (2) that the lens and pore ice remain continuous within themselves and are continuously connected, but the soil ice deforms dramatically to accommodate its movement or that of ice in the overlying lens.

In the first alternative one would assume that the ice fractures continuously as stresses build up in some way which tends to lift the growing lens away from the pore ice, as water flows into the base of the lens and freezes. However, as will be detailed further below, we note that all ice should be in a state of compression, and would therefore not crack. This is true of ice in the lens itself, because it must bear any overburden directly, and in any case it is compressed at least at the level of atmospheric pressure. Within the soil, ice is surrounded everywhere by water. Where it approaches soil mineral particles closely it will be in equilibrium with unfrozen films at elevated pressures. Where the ice-water interface occurs in unfrozen pores it is curved sufficiently so that a substantial pressure difference develops between the phases, with the ice at elevated pressure. To the extent that pore and lens ice are continuous, stresses will be continuous, and pore ice contiguous to the lens will be compresed at least to the degree that the lens ice is. Within the frozen fringe new lenses can only form when ice pressure builds to the point where it overcomes both the overburden and the cohesive effect of the unfrozen pore water. Whenever progressive freezing (increase in I) is occurring, the evolution of pressure in the fringe is in this direction. The formation of segregated ice is only evidence that pressures in one location have exceeded those confining the system, while pressures throughout the fringe have developed similarly, but to a lesser extent. These pressure relations are reflected in equations (3)–(7) above, which have been verified repeatedly. A more complete discussion of the unfrozen film–pore water–ice

equilibrium in relation to the elevated ice pressure may be obtained from the work by *Miller* [1980, chapt. 11].

In the second alternative to rigid ice regelation, one concedes continuity of the overall ice mass but must then assume large deformations on the part of pore ice as the growing lens heaves. This will be the case if one allows that the pore ice throughout the fringe will migrate, deforming or "flowing" around soil particles. It is also the case if one considers the pore ice in the fringe to be static on the whole but to deform continuously where ice forms near the base of a growing lens. Examination of relations between stress and strain rate for relatively warm ice illuminates this proposition. To estimate a microscopic ice strain rate we note that a reasonable ice velocity is the macroscopically observed heave rate, V_I, and we assume that a change in velocity on this order must take place over approximately the dimension of a soil particle, δ. This is, in fact, a generous assumption, because it is likely that such a change in ice velocity would have to occur sometimes over approximately a pore diameter, which is substantially smaller than δ. Thus a generous (small) order of magnitude estimate of the strain rate will be V_I/δ. If we consider silt size particles, then δ will be on the order of 10^{-6} m. A significant heave rate can be taken as at least one millimeter per day, or about 10^{-8} m/s. These figures provide an estimate of 10^{-2}/s for the order of magnitude of microscopic strain rate. It is unlikely that this number could be considered to be smaller for common situations of active heave and in a great many cases would probably be one or two orders of magnitude higher, due either to higher V_I values or smaller effective δ values. The important point is that strain rates on this order are quite unrealistic, even for ice near the melting point. To be specific, we refer to the experimental stress-strain rate relations displayed by *Mellor and Testa* [1969]. Their data show ice strain rates at 0°C increasing with stress, from the order of 10^{-7}/s at about 0.1 atmosphere to the order of 10^{-6}/s at about 10 atmospheres. Given continuity between pore and lens ice, we may use typical overburden pressures as the order of magnitude of the pore ice stress. It is doubtful that any overburden of interest would exceed 10 atmospheres, if only because such a pressure would suppress heave to a point below the level of practical interest. Thus ice strain rates required are unrealistically high by many orders of magnitude, if one assumes that growth of segregated ice or ice movement is accommodated by microscopic ice deformation.

Relations Between Variables

Our goal is to develop, solve, and explore a mathematical formulation of the phenomenon described above. Our strategy will be to develop relations between key variables so that they and the subsequently developed transport equations and side conditions may all ultimately be cast in terms of temperature and liquid pressure. Except where designated otherwise, these relations and the macroscopic variables in them pertain only to portions of whole noncolloidal soil, with or without ice present. Thus the central equations are applied directly only to the frozen fringe and the unfrozen zone, with linkage to contiguous zones and to external forces provided by various side conditions.

We assume that the processes involved are sufficiently slow and the contact between phases sufficiently pervasive so that local thermal equilibrium between the phases is achieved. As mentioned above, when hysteresis is not considered (which is reasonable when only freezing but no thawing is treated) there will be a unique relation between W or I and the phase pressure difference, in particular

$$I = I(u_i - u_w) = I(\phi_{iw}) \tag{8}$$

In general, as the ice content increases, the ice invades smaller pores and interstices, the radii of curvature of the microscopic phase interface decrease, and the pressure difference ϕ_{iw} increases. Substituting (6) in (8) yields

$$I = I(Au_w + BT) \tag{9}$$

where A and B are known constants, representing the coefficients which appear on the right-hand side of (6). (Note: A and B as used here differ from those used by *O'Neill and Miller* [1982] by a factor of ω_{iw}). For calculational purposes, relations of the form (8) and (9) must be determined experimentally or must be estimated on the basis of related experimental observations.

As noted above, utilizing a relation between phase contents and difference in phase pressures is the same kind of thinking which has been applied successfully to unfrozen, unsaturated granular soil. However, we emphasize that use of the analogy between freezing and drying of soil must be applied with care. For example, in the freezing case neither u_w or T alone may be related uniquely to W or I; nor can phase composition be related uniquely to either of u_w or u_i alone. This contrasts with the situation in above freezing soil, where a drying curve may be used to relate W and u_w uniquely, assuming passive conditions in the soil air. To put it another way, in the saturated freezing case the ice is not "passive" in the sense that high, spatially variable pressures may develop in it relative to the liquid. Here, one cannot specify u_i a priori in the way that one may assume ambient or other uniform values for soil air pressure. Rather, u_i will vary in space and time depending on transient conditions. This may even occur when there is negligible overburden or confining pressure. Tension in the unfrozen water provides a cohesive force, tending to hold the system together against the elevated pressures in the ice. Just as enormous pressure differences may easily develop between air and water in drying unfrozen soil, relative to atmospheric pressure, so here too very large differences between the phase pressures are likely to occur. Relations of the form (8) and (9) may be used to express the difference between u_w and u_i in terms of I (or W), but cannot alone locate that difference in terms of specific values of those individual pressures. Beyond this, none of the results discussed above pertains to freezing of unsaturated soil. These distinctions have not always been observed in frost heave modeling efforts. See *Miller* [1980] and *O'Neill* [1983] for further discussion.

For subsequent use we note the following differential relationships based on the foregoing:

$$\begin{aligned} dI &= \left(\frac{\partial I}{\partial u_w}\right)_T du_w + \left(\frac{\partial I}{\partial T}\right)_{u_w} dT \\ &= \left(A\frac{dI}{d\phi_{iw}}\right) du_w + \left(B\frac{dI}{d\phi_{iw}}\right) dT \\ &= AI'\, du_w + BI'\, dT \end{aligned} \tag{10}$$

where I' represents $dI/d\phi_{iw}$.

Transport Equations

Balance of mass over each water phase in a representative elementary volume of soil is expressed by

$$\frac{\partial}{\partial t}(\rho_w W) + \frac{\partial}{\partial x}(\rho v)_w = -S \tag{11a}$$

$$\frac{\partial}{\partial t}(\rho_i I) + \frac{\partial}{\partial x}(\rho v)_i = S \tag{11b}$$

where v_w and v_i denote volumetric liquid and ice fluxes, respectively, (m^3 H_2O/m^2 soil/s), and S is the rate of freezing (kg ice/m^3 soil/s). If there is no phase change, flow in each phase is governed by the familiar form flow equations given by (11) with the right-hand sides equal to zero. Phase change functions like a source-sink action, from the point of view of either phase alone. Given the rigid, saturated system, the rate of mass loss by one phase must be equal to the rate of gain by the other.

Conservation of mass of both water phases together is expressed by the sum of these equations:

$$\frac{\partial}{\partial t}[\rho_w W + \rho_i I] + \frac{\partial}{\partial x}[(\rho v)_w + (\rho v)_i] = 0 \tag{12}$$

Because both phases are considered together in (12), the rate of phase change does not appear explicitly but affects the values of individual components of the equation.

To reduce the number of unknowns in (12) we bring to bear some additional relations. The similarities between partially frozen and partially dried soil suggest that we apply a Darcy type flow law for liquid flux

$$v_w = -\frac{k}{\rho_w g}\left(\frac{\partial u_w}{\partial x} - \rho_w g\right) \tag{13}$$

where x is positive downwards, g is the acceleration of gravity, and $k(W)$ (meters per second) is the hydraulic conductivity. In the unfrozen zone, k is simply equal to the saturated hydraulic conductivity.

In keeping with the rigid ice assumption

$$v_i = V_I I \tag{14}$$

where V_I (meters per second) is the ice velocity (rate of heave) and is constant in space but variable in time. Substitution of (2), (13), and (14) into (12) yields

$$(\rho_i - \rho_w)\frac{\partial I}{\partial t} - \frac{\partial}{\partial x}\left[\frac{k}{g}\left(\frac{\partial u_w}{\partial x} - \rho_w g\right) - \rho_i V_I I\right] = 0 \tag{15}$$

Use of (10) eliminates derivatives of I:

$$(\Delta\rho A I')\frac{\partial u_w}{\partial t} + (\Delta\rho B I')\frac{\partial T}{\partial t} - \frac{\partial}{\partial x}\left[\frac{k}{g}\left(\frac{\partial u_w}{\partial x} - \rho_w g\right)\right] + \rho_i V_I\left[A I'\frac{\partial u_w}{\partial x} + B I'\frac{\partial T}{\partial x}\right] = 0 \tag{16}$$

where $\Delta\rho$ denotes $\rho_i - \rho_w$. Thus we obtain a mass flow equation with unknowns u_w, T, and V_I.

To obtain an applicable heat transfer equation we begin by writing

$$\sum(\rho c\theta)_n \frac{\partial T}{\partial t} + \frac{\partial q}{\partial x} = LS \tag{17}$$

where θ_n is the volume fraction of the nth component including soil solids, q is the conduction heat flux ($J/m^2/s$), and c_n is the sensible heat capacity of the nth component J/kg/°K and all soil components are included in the summation. It is difficult to obtain a truly rigorous derivation of such an equation for multiphase porous media, although many attempts have been made (see discussion by *O'Neill* [1983]). Nevertheless, (17) certainly has some precedence in the literature [e.g., *Fuchs et al.*, 1978]. Basically, the equation says only that changes in sensible heat content account for part of the divergence of q, the rest being balanced by the source-sink action of phase change. Because the rates of flow are slow, convection of sensible heat is neglected.

A Fourier heat conduction type law will be used to reexpress q

$$q = -K_h \frac{\partial T}{\partial x} \tag{18}$$

where K_h (J m^{-1} s^{-1}°K^{-1}) is the thermal conductivity of the whole soil. Equations (11*a*) or (11*b*) may be used to reexpress S, there being no obvious reason to choose one over the other. We will use (11*b*), which together with (14), (17), and (18) yields

$$\sum(\rho c\theta)_n \frac{\partial T}{\partial t} - \frac{\partial}{\partial x}\left(K_h \frac{\partial T}{\partial x}\right) - \rho_i L\left(\frac{\partial I}{\partial t} + V_I \frac{\partial I}{\partial x}\right) = 0 \tag{19}$$

Use of equation (10) to eliminate derivatives of I provides the governing heat equation sought:

$$[\sum(\rho c\theta)_n - \rho_i L B I']\frac{\partial T}{\partial t} - \rho_i L A I'\frac{\partial u_w}{\partial t} - \rho_i L V_I\left[A I'\frac{\partial u_w}{\partial x} + B I'\frac{\partial T}{\partial x}\right] - \frac{\partial}{\partial x}\left(K_h \frac{\partial T}{\partial x}\right) = 0 \tag{20}$$

CALCULATION OF V_I

The coupled heat and mass transfer equations have been reduced to two differential equations (16) and (20) in u_w and T. In principle, the system can be solved, provided that V_I is accounted for and that appropriate initial-boundary conditions and physical parameters are specified. Linkage of V_I to the solution system is a different matter from the straightforward specification of parameters and side conditions. This is because an independent balance must be drawn up to solve for V_I in terms of the variables in (16) and (20), while V_I appears simultaneously in those equations.

We have investigated two methods of calculating V_I, each based on mass conservation. Simple expressions are obtained, and we avoid redundancy with the general mass balance equation (16) because (1) balances are drawn up either only over the lens-fringe interface at x_b, or over the entire frozen fringe and unfrozen zone to the warm boundary at $x_w(x_b \geq x \geq x_w)$; and (2) in either case, we take advantage of our knowledge that the warmest lens consists of pure ice, moving at a rate of V_I.

To construct a mass balance at the plane through x_b we note that mass flux on the lens side of x_b is simply equal to $\rho_i V_I$. Immediately on the frozen fringe side of x_b, unfrozen water flows into the lens (freezes) at a rate of $(\rho v)_w$, while soil ice also moves into the lens with velocity V_I over a cross section I. The plane at x_b cannot itself accumulate mass; thus the total mass flux on one side must equal that on the other:

$$\rho_i V_I = \rho_i I V_I + (\rho v)_w \qquad x = x_b \tag{21}$$

When this relation is rearranged using (13) we obtain an expression for V_I

$$V_I = -k\left(\frac{\partial u_w}{\partial x} - \rho_w g\right)\Big/\rho_i g(1 - I)) \qquad x = x_b \tag{22}$$

The quantities on the right-hand side are evaluated at x_b and are determined from u_w and T as provided by concurrent solution of the transport equations. Values of V_I obtained from (22) apply wherever there is ice, however, because we have assumed that all ice is rigidly interconnected. It is interesting to note that (21) also provides a ratio of the flux of

ice to that of water into the base of the lens, namely, $I/(1 - I)$. Thus if I is on the order of $\frac{1}{3}$, ice flux into the lens is responsible for about one half the mass flow into the base of the lens.

A second means of calculating V_I derives from a mass balance over the entire length of whole (lens free) soil. The total mass flux through the plane at x_b is given by $\rho_i V_I$, while the mass flux at the warm end of the column is given by $(\rho v)_w$, as evaluated at x_w using (13). The difference between these two fluxes must equal the rate of change of the aggregate mass content inbetween

$$\rho_i V_I - \rho_w v(x_w) = \frac{d}{dt} \int_{x_b}^{x_w} [\rho_w W + \rho_i I]\, dx \tag{23}$$

This equation assumes that x increases in the direction of the warm end; otherwise, the terms on the left-hand side are reversed. We keep the warm end position (x_w) fixed over time with respect to the coordinate system. Although the point x_b is recurrently shifted at the instant when new lenses form (see below), it does not change at all other times, for which we may rewrite (23) as

$$V_I = \frac{1}{\gamma_i} v(x_w) + \frac{\Delta\rho}{\rho_i} \frac{d}{dt} \int_{x_b}^{x_w} I\, dx \tag{24}$$

The factor $v(x_w)$ may be evaluated from (13) on the basis of the current pressure solution. When u_w and T solution values are used to evaluate the integral at two successive points in time, [illegible] difference expression. Our previously reported results [*O'Neill and Miller*, 1982] used (22) to obtain V_I. However, all our more recent simulations are based on (24), for computational reasons to be explained below.

Application of Physical Conditions and Specification of Parameters

Boundary Conditions

Boundary conditions at the warm end of the column are determined from the physical situation there in a straightforward manner: water pressure or flux provides information in u_w, and temperature or heat flux provides information in T. Conditions at the cold end (i.e., at x_b) draw into play the distinctive physical character of that interface. Two conditions are needed, and these are provided by heat balance at x_b and by consideration of relations between mechanical forces there.

Considering mechanical forces we note that the pore ice and lens ice are continuous across x_b, and hence the ice pressure is as well. If we specify the overburden P, the weight per area which the x_b plane must bear, then u_i in both the lens and soil equals P there. We obtain a relation between u_w and T by substitution of P for u_i is the combination of (3) and (6):

$$P = (1 + A)u_w + BT \qquad x = x_b \tag{25}$$

If one constructs a heat balance across x_b in much the same manner that mass balance was used to obtain (22), then the remaining necessary coldside boundary condition is obtained. We assume that material on the cold side of the warmest lens is relatively inert, in the sense that heat is conducted through it but insignificant additional phase change occurs there. In addition, we assume that the freezing process is slow enough so that a quasi steady temperature profile exists there, changing only as phase composition, length, or boundary temperatures change. This assumption is a computational convenience to expedite exploration of the central features of the model, and could be discarded without affecting any major points in the theory or practices we have employed. On the warm side of the lens, heat conduction through the soil is given by (18). Beyond this, latent heat is transported through the soil on the warm side into the base of the lens by the flow of unfrozen water. All this flow is intercepted by the lens. In other words, the liquid flux into the lens times the latent heat of fusion equals the rate of liberation of latent heat due to freezing at x_b. Thus a heat balance at x_b dictates

$$K_{hf}\left(\frac{T_b - T_c}{l}\right) = K_h \left.\frac{\partial T}{\partial x}\right|_{x_b} - L(\rho v)_w|_{x_b} \qquad l = x_b - x_c \tag{26}$$

where K_{hf} is the thermal conductivity of the entire frozen zone on the cold side of x_b, T_b the temperature at x_b, T_c the temperature at the cold external surface at x_c, and $l(t)$ is the length of the frozen zone from the cold external soil surface to x_b. This equation simply says that the jump in conduction heat fluxes across x_b is proportional to the rate of freezing there. The last term in (26) may be reexpressed using (13).

Equations (25) and (26) contain relations and nonlinearities in both u_w and T and are included simultaneously with the governing transport equations in solution procedures. Initial conditions in u_w and T depend on the case considered and are described below for various specific simulations.

Lens Initiation and the χ Parameter

In what has preceded, equations have been discussed which apply to processes in the whole soil, that is, in the zone from the warm end of the column (x_w) to the warm side of the warmest lens (x_b) within the frozen fringe. As freezing progresses and ice pressure builds, conditions somewhere within the fringe may dictate that a new lens will form. Beginning as a mere sliver, this new lens becomes the warmest lens, growing larger as it intercepts and freezes the flow of liquid which formerly terminated at the old warmest lens. With continued freezing, the process may be repeated. The inception of new lenses occasions a recurrent relocation of the reference point x_b and is a fundamental feature of the physical processes to be simulated.

To determine when and where a new lens will be initiated we must monitor the pressure situation as (16) and (20) are solved through time. An ice lens will bear the full load being lifted by heave, but to initiate a new ice lens from pore ice in the fringe, pore ice pressure must exceed ice pressure in the lens. That is, the ice stress must offset the fact that the effective load is augmented by the cohesive action of surface tension and by residues of capillary water at a pressure less than that of the ice, perhaps very much less. Clearly, if particles are to move apart as a new lens is initiated, at that location no stress is transmitted through intergranular contacts in the soil skeleton, and the overburden P must be balanced by the pore contents alone. The net stress over a cross section of soil provided by the pore contents will be some weighted average of the higher stress in the ice and the lower stress in the water. The moment ice enters a gap left by a broken intergranular contact, the required ice pressure is diminished; the low-pressure water will have been replaced by ice. Hence the crucial location for lens initiation ought to be at the boundary of a large ice-filled pore. The analogue of this is the replacement of low-pressure water by air when moist soil cracks, a problem that can be translated into one of tensile failure of a flawed medium in which the average effective stress is known [*Snyder*, 1980; *Snyder and Miller*, 1985]. Snyder and Miller found that this approach, using *Aitchison*'s [1961] formula for

estimating average effective stress, provided a reasonable fit to data in tensile strength of moist soils.

Although the above mentioned work was done in terms of unfrozen unsaturated soil, we may translate it to the ice-water case. As we have noted in connection with the results of *Koopmans and Miller* [1966], there are certain similarities between freezing and drying. In particular, at a given value of W for a given granular soil one will find the same microscopic configuration of pore phases in desaturating, unfrozen soil on the one hand, and freezing saturated soil on the other hand. This implies the same relative apportioning of stress between the two pore phases in either case. Thus we express the total pore stress, or "neutral" stress σ_n as

$$\sigma_n = \chi u_w + (1 - \chi)u_i \tag{27}$$

where $\chi(W)$ is a weighting factor evaluated in accordance with the results of Snyder and Miller. They concluded that the appropriate formula for χ would be obtained, when the effective (intergranular) stress goes to zero, if a summation formula proposed by *Aitchison* [1961] is multiplied by 0.5. They also provided a theoretical basis for this adjustment. When the summation formula is converted to an integral in terms of unfrozen water content W, then χ is given by

$$\chi(W) = \frac{0.5}{n}\left[W - \frac{0.3}{\phi_{iw}(W)}\int_W^n \phi_{iw}(\omega)\, d\omega\right] \tag{28}$$

where n is the porosity, and ω is a dummy variable of integration corresponding to W. Given a relation between ϕ_{iw} and W, this may be evaluated by quadrature. Alternatively, one may use the function $I'(\phi_{iw})$ required elsewhere (i.e., in equations (16) and (20)) to transform the integral to

$$\chi(W) = \frac{0.5}{n}\left[W - \frac{0.3}{\phi_{iw}}\int_W^n \phi_{iw} I'\, d\phi_{iw}\right] \tag{29}$$

As work on this simulation system has progressed since the reporting of preliminary results [*O'Neill and Miller*, 1982], the overall theory has remained unchanged, but the particular computational strategies and parameter representations have evolved in the direction of greater realism, relevance, efficiency, and accuracy. The computed results to be presented below span a time period over which this evolution took place. Rather than belabor the details of parameter identity and calculation for each computed case, we will describe the most recently used and presumably best formulations, with occasional indications of the course of development. Alterations in computational strategy and parameter values changed computed results to some degree but have no real bearing on the qualitative nature of our findings. It is the general character of the computed results, not the specific numerical values which we wish to stress in this paper.

In the case of the χ representation, our preliminary results were based on the formula

$$\chi = \left(\frac{W}{n}\right)^{1.5} \tag{30}$$

which reflects a very approximate attempt to portray Snyder's early measurements. Subsequently, this representation was upgraded to the equivalent of (29) with the integral neglected. In the most recent runs the full equation (29) was used and was evaluated analytically.

Physical Parameters in the Transport Equations

Ideally, for testing purposes, one would like to obtain $W(\phi_{iw})$ (and hence I') as well as $K_h(W)$ and $k(W)$ from the same sample of soil under controlled conditions identical to those in the physical heave experiment to be simulated. Unfortunately, this is an extremely challenging proposition. Results obtained for some of these quantities with a number of soils have been published, together with a discussion of uncertainties that have yet to be eliminated [*Horiguchi and Miller*, 1980, 1983].

For the present we use a curve for W obtained from a semilog regression on lab data for a silty soil used in physical tests in which heave was induced and recorded. This W curve (Figure 2) was obtained by desaturating unfrozen samples of the soil. By virtue of the findings of *Koopmans and Miller* [1966] mentioned above, it has been scaled in accordance with (7) and is taken to be representative of one which would be obtained in a freezing sequence. The solid line in the figure represents the regression curve fit in the form

$$W = \sum_{k=0}^{5} A_k(\ln \psi)^k \qquad \psi = \phi_{iw}/\omega_{iw} \tag{31}$$

where the A_k are constants determined by the regression. This series can be differentiated analytically to produce I', which may be used in turn in the governing equations (16) and (20) as well as in (29), where the integral may now be evaluated analytically.

The hydraulic conductivity k has been specified throughout this work as

$$k(W) = k(n)\left(\frac{W}{n}\right)^{\gamma} \tag{32}$$

where n is the porosity, and γ is a negotiable constant. Noting again the similarity of liquid phase configurations during unfrozen drying and saturated freezing, we originally assigned γ a value of 7 on the basis of previous work by *Bresler et al.* [1978] on unsaturated flow. In more recent runs, γ was changed to 9, reflecting admittedly sparse measurements made directly on samples of frozen silt. Work on the measurement of this crucial parameter continues in the laboratory of the second author.

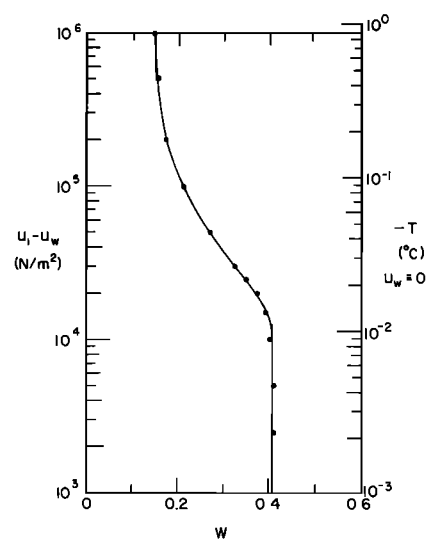

Fig. 2. Unfrozen water content (W) versus temperature if u_w is held at zero, or alternatively, versus u_i-u_w.

Thermal conductivity is also a function of phase content. Once heave is underway the frozen zone ($x_c > x > x_b$) consists of segments of pure ice interlayered with segments of frozen soil. Thus K_{hf} was evaluated using a "composite wall" type formula for equivalent (effective) conductivity:

$$K_{hf} = \frac{l}{\int_{x_c}^{x_b} \frac{dx}{K_h}} = \frac{l}{\frac{h}{K_{hi}} + \frac{l-h}{K_{hs}}} \tag{33}$$

where $h(t)$ (m) is the cumulative heave (sum of the thicknesses of all ice lenses), K_{hi} is the thermal conductivity of pure ice (2.32 W m °K), and K_{hs} is a representative value of the thermal conductivity of frozen silt (2.93 W m °K). In the frozen fringe the geometric mean formula was used (see, for example, *O. Johansen*, [1977])

$$K_h = K_{hi}{}^I K_{hw}{}^W K_{hm}{}^G \tag{34}$$

where K_{hw} is the thermal conductivity of pure water (0.58 W/m/°K), and K_{hm} the thermal conductivity of a solid sample of the soil minerals. In the limited number of cases where its investigation is documented in the literature, the formula (34) has been found reasonably adequate. When applied to data for partially frozen soils as presented by *Penner* [1970] the formula performs quite well.

The overall soil sensible heat capacity was calculated as the simple volumetrically weighted sum of the component values, those being estimated from typical published values. Ice and liquid water values are well known, and, on a volumetric basis, values for soil minerals vary little for different mineral contents [*deVries*, 1963]. In any event, in the cases investigated sensible heat effects were usually not very significant.

NUMERICAL METHOD

The governing equations (16) and (20) were solved by the Galerkin finite element method. Full details of the rather involved solution procedures will not be given here. While standard texts [e.g., *Pinder and Gray*, 1977] provide a basic explanation of the method used, space does not permit exposure here of full details of the rather involved solution procedures necessitated by the complexity of the calculations with all their contingencies. Hence only an outline of our method is presented below, with indications of some particulars so that one gains some notion of how the nonlinearities were dealt with.

In brief, the variables u_w and T were approximated by the series

$$u \approx U_k(t)\Omega_k(x) \qquad T \approx T_k(t)\Omega_k(x) \qquad k = 1 \rightarrow N \tag{35}$$

where the set of T_k and U_k are time-dependent coefficients to be sought. The Ω_k are preselected basis functions which interpolate the solutions over space; N is a finite number, and the repeated subscripts indicate summation over the range of k. Piecewise linear interpolation functions Ω_k were used, which means that U_k and T_k correspond to dependent variable values at the node points. Using usual Galerkin finite element procedures in each governing equation, one obtains $2N$ algebraic equations in the $2N$ unknown coefficients, T_k and U_k. Each (jth) algebraic equation is of the form

$$C_{jk}\frac{dU_k}{dt} + D_{jk}\frac{dT_k}{dt} + E_{jk}U_k + F_{jk}T_k + R_j = 0 \qquad j = 1, 2, \ldots, N \qquad k = 1 \rightarrow N \tag{36}$$

We apply (36) at successive points in time, t', where $t_m \leq t' \leq t_{m+1}$, and where the dependent variable values are known at t_m and unknown at t_{m+1}. That is, we write

$$U_k(t') \approx \varepsilon U_k{}^{m+1} + (1-\varepsilon)U_k{}^m \tag{37}$$

and similarly for $T_k(t')$, where ε is a numerical parameter dictating the degree of implicitness in the differential expressions. Use of (37) and approximation of the time derivatives in the manner of

$$\frac{dU_k}{dt} \approx \frac{U_k{}^{m+1} - U_k{}^m}{t_{m+1} - t_m} \tag{38}$$

allows us to rearrange (36) in the form

$$[G]\{Y^{m+1}\} = [H]\{Y^m\} - \{R\} \tag{39}$$

$$\{Y\} = \begin{bmatrix} U_1 \\ T_1 \\ \cdot \\ \cdot \\ \cdot \\ U_N \\ T_N \end{bmatrix}$$

where the matrices $[G]$ and $[H]$ contain the time step size, ε, V_I, and various physical coefficients dependent on u_w and T.

The equations are quite strongly nonlinear via I' and $k(W)$, which are evaluated iteratively using an under relaxation scheme. That is, the physical coefficients are evaluated iteratively from the solution Y^* where,

$$Y_k{}^* = \alpha Y_k{}^{m+1} + (1-\alpha)Y_k{}^m \tag{40}$$

The numerical parameter α was kept less than ε, and Y^{m+1} on the right-hand side signifies the new values obtained from the latest iteration. Numerical experiments suggested that an acceptable balance of accuracy and stability was obtained with ε and α equal to 0.75 and 0.5, respectively. Those values were used in all runs after the preliminary ones.

V_I was evaluated iteratively using Y^* for the pressure solution to obtain $v(x_w)$ in (24). The integral in (24) was calculated at t_m using Y^m and at t_{m+1} using the latest iteration for Y^{m+1}, with Simpson's rule applied over each element. Finite differencing in the manner of (38) was used to obtain the integral's time derivative. The boundary conditions (25) and (26) were included simultaneously in the algebraic system symbolized by (39), with (25) written at t_{m+1} and (26) formulated at a time corresponding to Y^*. Because solution values over the whole extent of the frozen fringe determine the integral in (29), the banded nature of the system (39) would have been destroyed if the equation for V_I had been included simultaneously, instead of iteratively.

COMPUTED RESULTS

The Course of a Simulation

In every case, the soil column was considered to be initially unfrozen over most or all of its length. In the preliminary runs the initial temperature in a 15.3 cm column was 1.0°C, with the warm end kept at that temperature throughout. The cold surface at x_c was ramped gradually down to −0.5°C and then held there. Results from these runs are reported by *O'Neill and*

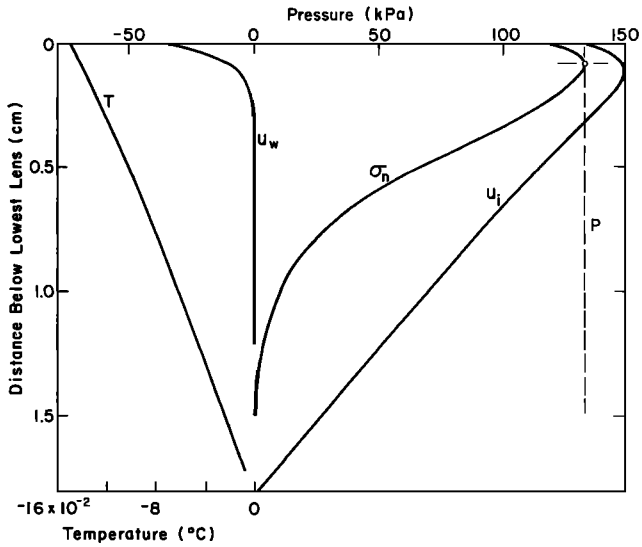

Fig. 3. Computed profiles in T, u_w, u_i, and σ_n across the frozen fringe at the moment when σ_n surpasses P.

Miller [1982]. The gradual cooling sequence illustrates the role of the boundary condition (25) and the consequences of the physical ideas behind it. With the initial cooling, the expansion of water on freezing drives the liquid pressure in the column up, with the ice pressure at a higher level yet. Liquid is forced out of the warm end of the column. The pressures may build up until heave results, which serves to limit or relieve the build up in total pore pressure at a level dictated by the values of P. The boundary condition (25) may be rewritten as

$$u_w = \frac{P - BT}{1 + A} \qquad x = x_b \tag{41}$$

As freezing continues and T drops at x_b, the value of P (equal to the ice pressure) remains fixed while the value of u_w is forced down, in accordance with (41). This depression of u_w at the cold end of the fringe motivates the liquid flow through it and into the lens, furnishing the mass transport needed for heave to occur. These heaving mechanisms serve to relieve σ_n, ensuring that it cannot exceed the pressure P which confines the specimen.

Figure 3 shows typical calculated dependent variable profiles across the frozen fringe, at an instant when a new lens is about to form. The widening of the gap between u_i and u_w is evident, as one looks toward the more frozen end of the fringe. In accordance with the processes discussed above, the value of u_w drops rather precipitously near the base of the lens, which lies at the top of the figure. At the moment depicted in Figure 3, σ_n at its maximum point has just surpassed P, and thus a new lens will form there. Computationally, this means that the numerical mesh will be shifted downward, relocating x_b at the base of the new lens, with values at the new node points interpolated from the previous mesh. Boundary conditions are reapplied at the new x_b, and the process repeats itself.

One onus of our modeling system is its dependence on calculating the inception and growth of each lens. Especially under certain conditions including rapid freezing, the lenses formed can be veritably microscopic, with commensurately small segments of frozen soil between them. It is gratifying that the model predicts this under the kind of conditions where this phenomenon is observed in the laboratory. However, this requires a great deal of computation. The problem might be alleviated by skipping the calculation of whole groups of consecutive fine lenses, assuming that the character of each group may be interpolated from a sampling of lens computations on each side of the group. The spacing of lenses depends upon the characteristics of the soil, as well as on applied conditions. During later runs than the one producing Figure 3, a more realistic $W(\phi_{iw})$ function was used (i.e., Figure 2), producing more generous lens spacings.

Catching the moment when σ_n surpasses P also poses a computational challenge. We have dealt with this by having the program determine time step sizes so that σ_n should not surpass P greatly (on a percentage basis) during any one time step. When P is surpassed, the last time step is shortened and recalculated. Various interpolation and iteration schemes were then used to zero in on the moment when the surpassing occurred. The purpose of these procedures was to terminate simulation of the growth of a given lens when a new lens had formed, intercepting liquid flow to the old lens. In general, other things being equal, the slowdown of freezing brings greatly increased time lapses between successive lens formations. After the inception of each new lens, the time step was reset as some fraction of the total elapsed time between inception of the current lens and of the previous one. In this way the temporal resolution of the computational system could always be geared to the evolving time scale of events in the heaving system.

Figure 4 shows the results of the simulation which produced the profiles in Figure 3. The shaded portions of the column represent ice lenses, which have formed in the kind of banded pattern observed in lab experiments. The larger lenses grow during the final stages of the freezing sequence, when ice penetration is nearing its limit and the contributing processes have slowed greatly. Under these conditions, it becomes increasingly easy for the suction generated in the frozen fringe to draw water through the soil at rates commensurate with the now reduced freezing requirements. In other words, it becomes easier to accomplish continued freezing by drawing unfrozen water into the fringe than it is for ice to penetrate new unfrozen interstices. Eventually, other things being equal, penetration will cease, and a terminal lens will form which will grow indefinitely as the system asymptotically approaches a quiescent state. The locus in time and space of this cessation of penetration depends in part on the freezing rate and load P which are imposed. In some cases with relatively low values of each it may occur very early, or there may be virtually no ice penetration at all. The terminal stage of heave has features which are qualitatively distinct from the other stages.

Analysis of the results of numerous runs showed that our simulations tend to become unstable during the terminal stage of heave. Under relatively high overburdens, the model could often be run for extended periods of time after penetration had ceased for all practical purposes. However, the lower the value of P, the more likely were stability problems during the terminal stage. This may be the result of some purely numerical problems or may reflect inadequate physics for the peculiarities of this ultimate stage, or both. Examination of details in the calculations produces circumstantial evidence that the difficulty centers around calculation of V_f and the effect of its value.

During the final stage V_f plays a much greater role in the calculations of heat balance in the frozen fringe than during earlier time. During initial relatively rapid freezing the phase change effects are dominated by the $\partial I/\partial t$ term in (19). However, when penetration becomes negligible, $\partial I/\partial t$ becomes very

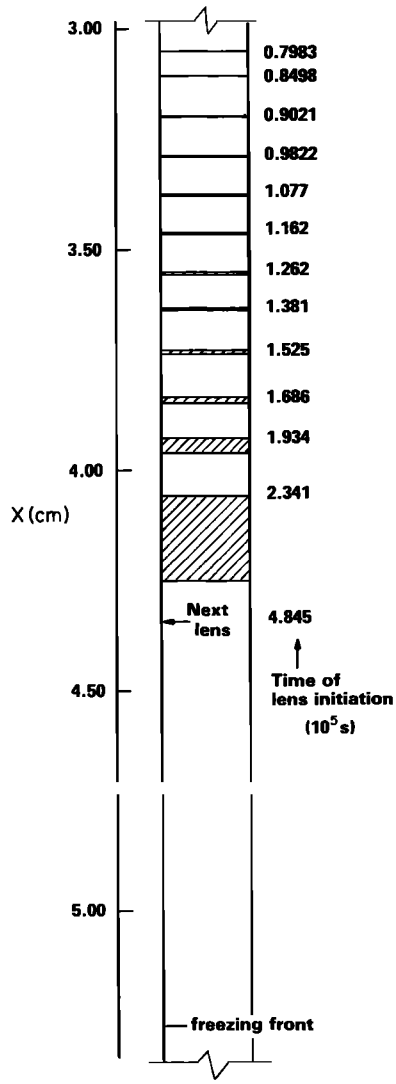

Fig. 4. A portion of a freezing soil column showing computed ice lens locations (shaded) and their times of initiation.

small. Essentially, all the phase change consists of conversion of all liquid inflow into ice outflow over a spatially steady frozen fringe. In terms of the equations, this means that the V_I term in (19) (and hence terms in the second line of equation (20)) becomes predominant in the phase change heat balance. At the same time, the calculation of V_I itself becomes more precarious at this stage. Because the ice content profile has become relatively steady, the time derivative of the integral in (24) is much reduced in significance. During earlier time, penetration proceeded with considerable momentum, which elevated the significance of the integral term. This in turn tended to buffer iterative or other fluctuations in the $v(x_w)$ term in (24). However, during the final stage, fluctuations or slight errors in the $v(x_w)$ term translate directly into errors in the V_I calculation. This translates through (20) into errors in T and hence in the phase change rate. Through mass balance, this translates iteratively into further errors in the $v(x_w)$ calculation. Use of (22) instead of (24) for determining V_I resulted in similar difficulties, exacerbated by the fact that key quantities in (22) are greatly dependent on the value of T at the single point x_b. The formulation based on (24) was related, by contrast, to fluctuations of the entire heat and mass balance over the column and hence was more stable.

Sensitivities and Qualitative Character of Results

It has been observed physically that increasing the magnitude of P tends to reduce heave, other things being equal. A series of step freeze simulations was undertaken to evaluate the model's sensitivity to variation of P, under conditions slightly different from those in the preliminary runs. In step freeze tests, T_c is lowered suddenly to a predetermined value and then held there while conditions at the warm end are held constant, as before. In this sequence of runs the initial temperature assumed over most of the column was 1°C, with an initial thin frozen zone including frozen fringe assumed at the cold end. T_c was set to −1°C at time zero, and an initial value of T_b was guessed either by solving (25) for T with u_w at zero (the initial condition in u_w) or by drawing on experience. In either case, the system rapidly adjusted T_b to a more consistent value, or, in a small number of cases, behaved erratically, in effect requesting a better first guess which was then provided.

Figure 5 shows computed heave histories obtained under these conditions for a 10-cm long column. Cumulative heave, h, was calculated from the numerical equivalent of

$$h(t) = \int_0^t V_I \, dt \tag{42}$$

The heave magnitudes and rates shown are believable in relation to lab observations and the model evidently responds appropriately to variations in P. An applied surcharge of 150 kPa supresses heave greatly, forcing a large degree of ice penetration into the soil. However, a load of 50 kPa hardly achieves ice penetration, with a large portion of the freezing associated with ice segregation. For the assumed soil characteristics, variations in P in the vicinity of 100 kPa produce the most visible alterations in the character of the heave histories. Thus for the particular soil and freezing sequence simulated we might regard the vicinity of 100 kPa as a critical zone for P.

Subsequent figures explore activity in this critical zone in more detail. Lab step freeze tests have sometimes shown heave occurring even while water is being forced out of the warm end of the column. In particular, this may occur during early time when freezing is rapid and the lenses formed are too small to see. The flow may then reverse subsequently, as freezing slows down, with intake of water eventually contributing significantly to the heave and visible lenses forming. This expulsion of water with flow reversal is more likely to occur under higher values of P (see, for example, *Penner and Ueda* [1977]).

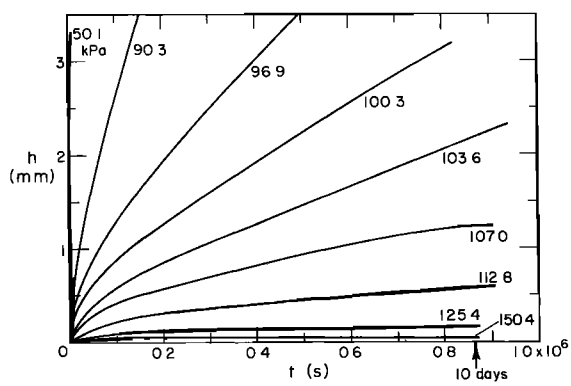

Fig. 5. Cumulative heave histories for various values of P.

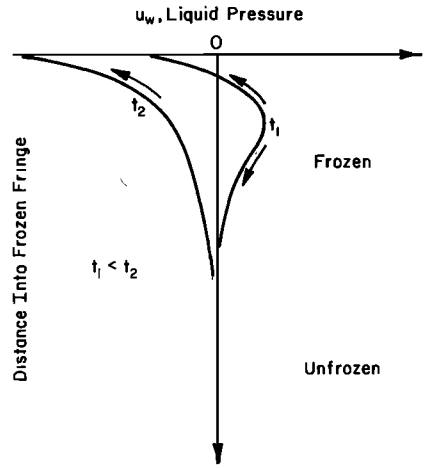

Fig. 6. Schematic depiction of water pressure profiles (u_w) in the frozen fringe at successive times before and after flow reversal with arrows showing the direction of liquid flow.

The explanation for this phenomenon is provided by the model in terms of pressure profiles illustrated schematically in Figure 6. During early time the rapidity of freezing and the expansion of water with phase change tend to drive up the pressure in the pore contents. This pressure is relieved at both ends of the column. Liquid is driven away from the zone of most active freezing, causing expulsion at the warm end while also contributing to heave at the colder end. Later, when freezing has slowed, the system "relaxes," so to speak. Liquid pressure is relatively depressed at x_b, and the reduced freezing rate means that the liquid pressure is more easily relieved throughout. Hence the u_w profile is negative everywhere, following the drop imposed at x_b. At this stage we witness an influx of water from the warm end, which eventually completely supplies the mass which accumulates as segregated ice.

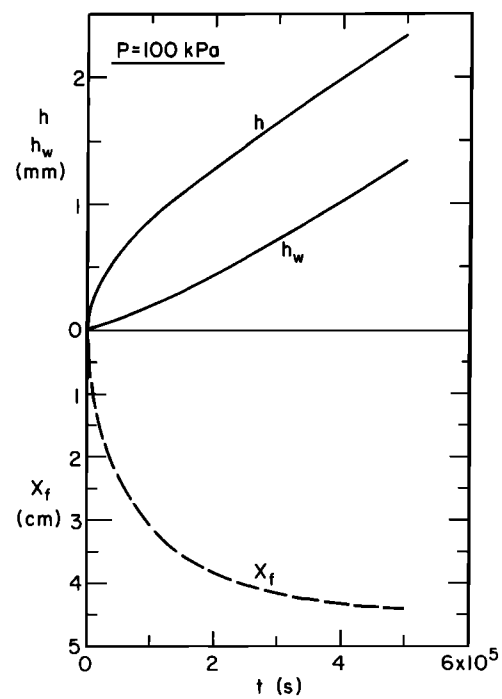

Fig. 7. Cumulative heave (h), heave due to water intake (h_w), and location of the freezing front (X_f) over time for a step freeze simulation.

Larger lenses form during this stage, because more freezing than before is associated with inflow than with expansion of water on freezing as ice penetrates. Each lens grows for a relatively long time, before increased freezing in the fringe can drive pressures there up enough to initiate a new lens.

Figure 7 shows results for a step freeze under a P of about 100 kPa, with h_w denoting the heave due only to water intake, i.e., due to the $v(x_w)$ term in (24). X_f denotes the location of the freezing front, arbitrarily taken as the point of 0.1 ice content, which might correspond to a visually identified front location. Initially, the h and h_w curves are not parallel, indicating that the expansion of water on freezing contributes quite significantly to the mass needed for heaving. On the right-hand side of the figure, near the limit of ice penetration, the two curves have become nearly parallel, reflecting the fact that the mass for nearly all additional heave is supplied by inflow from the warm end.

Figure 8 shows results from an identical run, except that the surcharge has been increased to about 107 kPa. Here the balance of factors has changed distinctly. During most of the period of active ice penetration, heave is almost totally achieved from the excess volume provided by the expansion of water on freezing. Relative to the magnitude of h, expulsion of water is substantial. However, as observed in lab experiments, this flow eventually reverses when the freezing rate has declined, in this case when ice penetration has nearly ceased. The h and h_w curves then become parallel, and most of the heave is associated with what is probably the terminal lens. We note that the model mimics lab observations in the pattern of initial outflow and flow reversal with high P and in the formation of veritably microscopic lenses during the initial stage of heave.

Figure 9 shows another effect usually associated with a decline in the freezing rate, namely, an increase in the ice segregation ratio (ISR). An ISR is a strainlike quality, which may be defined as the ratio of the total thickness of segregated ice within a segment of frozen soil divided by the current length of that segment. We will designate an overall or global ISR as that which pertains to the whole frozen zone, that is,

$$\text{ISRG} = h/l \tag{43}$$

The local ISR (ISRL) pertains to some particular subsection of the frozen zone, which, in the case of Figure 9, is the most recently frozen material. We may define the ISRL as

$$\text{ISRL} = V_l/(V_f + V_l) \tag{44}$$

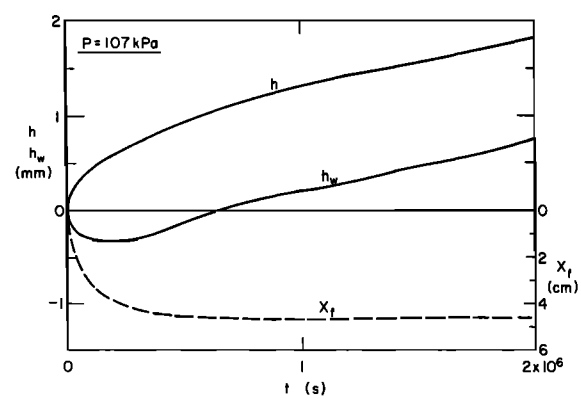

Fig. 8. Results from a step freeze simulation identical to that in Figure 7, but at a higher overburden, showing the flow reversal over time.

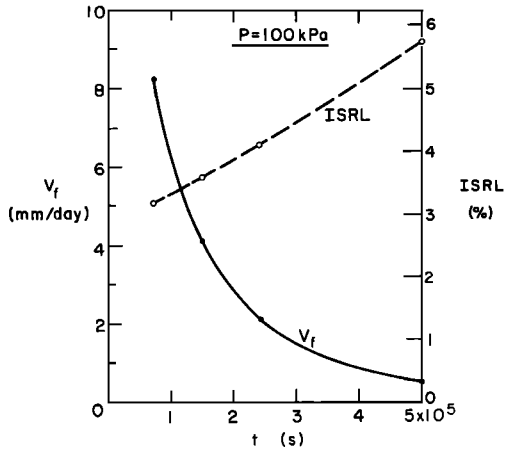

Fig. 9. Local ISR and freezing rate versus time for a step freeze simulation.

where V_f is the rate of progress of the freezing front X_f. In other words, the ISRL is the ratio of the rate of heave to the rate of elongation of the frozen zone. Alternatively, considering Figure 4, one can estimate the ISRL at any level in the column by taking the thickness of a lens and dividing it by the thickness of the lens plus the band of frozen soil immediately above it (and below the previous lens). The global ISR is appropriate for quantifying aggregate or cumulative effects, while the local ISR is useful for describing more limited segments of soil or current events during a longer evolution. The trend shown in Figure 9 corresponds to that seen in the laboratory, and the magnitudes of the quantities are reasonable.

To explore the model further, simulations were run on a much larger scale, more in line with field scale problems. A 35-m vertical column of soil was considered, with an initially hydrostatic profile in u_w. The sequence began with an assumed T_c on the upper surface of -5°C and a fixed temperature of 3°C at the 35 m depth. Liquid pressure at the warm end was held at the initial hydrostatic value, and the initial temperature was assumed to be 3°C throughout. Initial overburden on the freezing zone was taken as 50 kPa. For convenience it was also assumed that about 10 cm of solidly frozen material was directly beneath the top surface. These conditions were only intended to bear some resemblance to conditions beneath a cold buried pipe and to provide a framework for exploration of a large scale simulation.

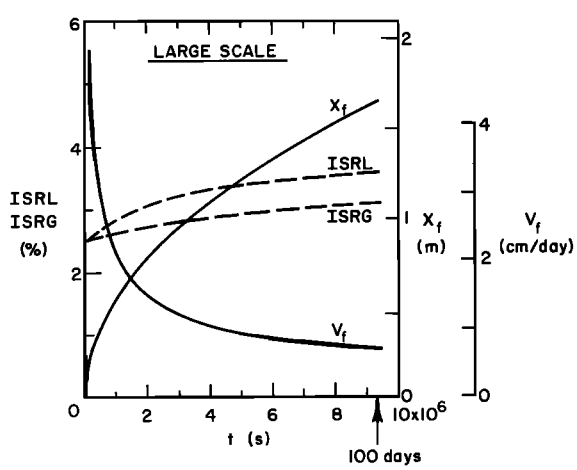

Fig. 10. Results from the first 100 days of a large-scale step freeze simulation.

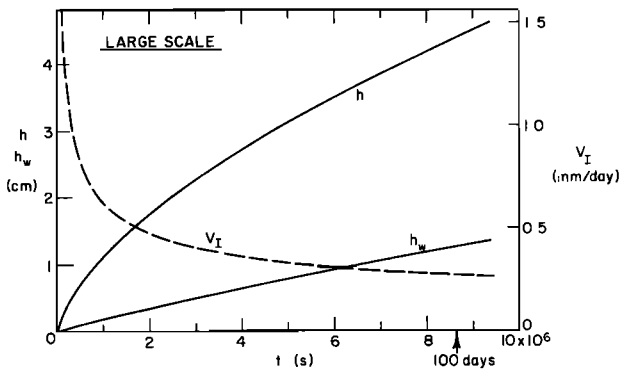

Fig. 11. Heave rate, cumulative heave, and heave due to water intake over the first 100 days of the large-scale simulation.

Figure 10 shows results from the first 100 days of this run. As in the small scale runs, we note that both ISR's increase with a declining V_f (ISRG being in effect a spatial integral of ISRL). However, we note that this effect moderates as time proceeds, with the ISR curves flattening out relative to that in Figure 9. Figure 11 shows h, h_w, and V_I versus time for this case, also during the first 100 days. During the early rapid freezing, V_I is relatively high as all contributing processes happen at a faster pace initially. However, the ISR's are still relatively low initially because frost penetration is still quite rapid. After the first 100 days. the h and h_w curves are still not tending toward parallel paths.

The behavior of the h and h_w curves in Figure 11 and of the ISR curves in Figure 10 are illuminated further in Figure 12 where the results from the first 1000 days of simulation are shown. Here the contrasts to the smaller scale, constant P runs persist, with evident cause: as the depth of freeze increases, the weight of overburden on the frozen fringe constantly increases. An interplay of rate dependent effects results, causing ongoing changes in relationships which stabilized in the smaller scale, constant surcharge cases. Also, the growth in P eventually suppresses heave so severely that despite declin-

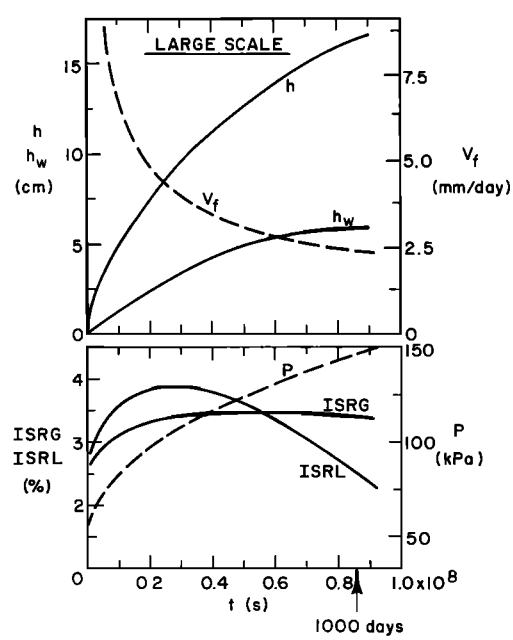

Fig. 12. Large-scale results over the first 1000 days showing a turn around in the ISRL curve with increasing P.

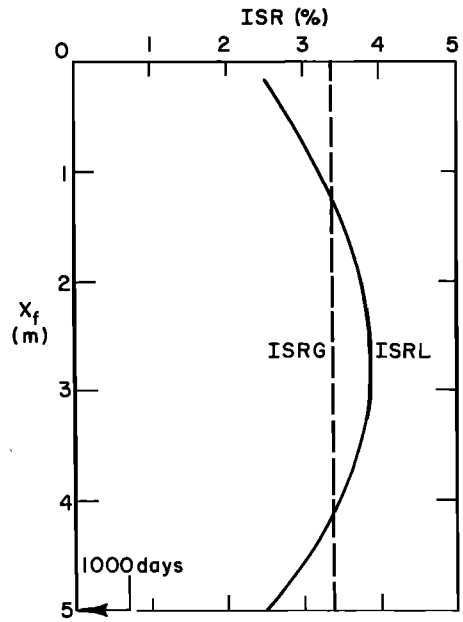

Fig. 13. Vertical profile of ISRL, with dashed line showing the ISRG at 1000 days for the large-scale simulation.

ing V_f, the ISRL peaks out such that the more sluggish ISRG curve ultimately turns around as well. This is illustrated spatially in Figure 13, where a vertical ISRL profile is shown. The ISRG is the global ISR one would detect on the soil surface at 1000 days, measuring the cumulative heave and knowing the depth of freeze. Despite many differences between the large and small scale cases, the development in both of about one atmosphere of overburden pressure severely suppresses heave. This neighborhood of the P value appeared to be a critical range in the small scale tests, and one notes that the ISRL peaks out when P achieves this magnitude on the large scale.

The last three figures contain results from additional small-scale runs, much like the previous ones except that here both column end temperatures decreased linearly with time ("ramp tests"). This was done to achieve steadier frost penetration and other rates. These runs were done for comparison to very preliminary lab data in a continuing series of such ramp tests undertaken to aid in design studies. All results shown are from the simulations, the curves being drawn from the points indicated. Some physical information was available to us, such as the curve in Figure 2 for a soil like that used in the lab. On the whole, however, we lacked definitive information on the soil characteristics such as would be needed for a strict test of the model. Also, the preliminary lab data were quite sketchy, possibly distorted by such factors as friction on the sides of the column containers. ISRG values are averages over the sections of frozen soil where V_I and V_f were most steady, typically over most of the ultimately frozen material.

Despite the limitations the results are gratifying. Simulated heave and ISR magnitudes were generally larger than those observed. However, the same trends appeared in each figure as in the lab data, with steeply rising ISRG at the left in Figures 14 and 15, and greater rise of V_I with V_f (Figure 16) for lower surcharges. Also, perhaps most importantly, both the lab tests and the simulations produce the same relative rankings of cases, in terms of heave rate and ISR versus the other factors.

SUMMARY AND DISCUSSION

This paper has explored the nature of a mathematical description of frost heave designed to simulate the coupled heat and moisture flow processes whereby segregated lenses of pure ice grow within the soil, thereby deforming the soil surface. The theory has been formulated for the case of incompressible soil, free of air, colloids, and solutes. Despite these constraints, the model has value as a first step towards a fundamental understanding of the underling mechanics of frost heave.

In constructing this model we have relied to the maximum extent on considerations of rational physics and thermodynamics of freezing soil, eschewing nonphysical correlations or any ignorance factors designed to swallow whole our lack of understanding for the convenience of the modeling exercise. The model rests primarily on (1) the central equations in temperature and liquid pressure, developed with reference to the basic conservation laws, and from fundamental thermodynamics (the Clapeyron equation); (2) experimentally supported concepts relating phase composition of the system, its state, and its capillarity; (3) rational criteria for pore stress partitioning and for what amounts to mechanical failure of the soil, when each new lens of segregated ice forms. A central feature of the model, which allows closure of the equations and facilitates their solution, is the rigid ice assumption. That is, we have relied heavily on the belief that soil ice tends to form on preexisting ice and thus grow through the pore system to form one solid body. This means that pore ice in the frozen fringe is solidly connected to lens ice, as both move toward the cold

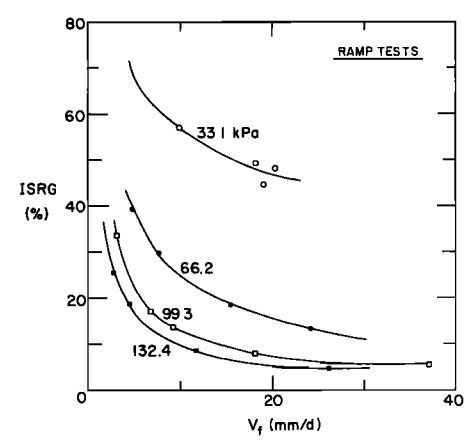

Fig. 14. Results from small-scale, ramp freeze simulations relating ISRG and freezing rate for different overburdens.

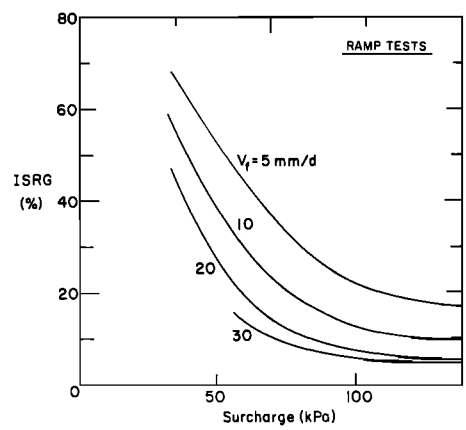

Fig. 15. Computed results for the same cases as in Figure 14 showing larger ISRG values at reduced overburden and reduced freezing rates.

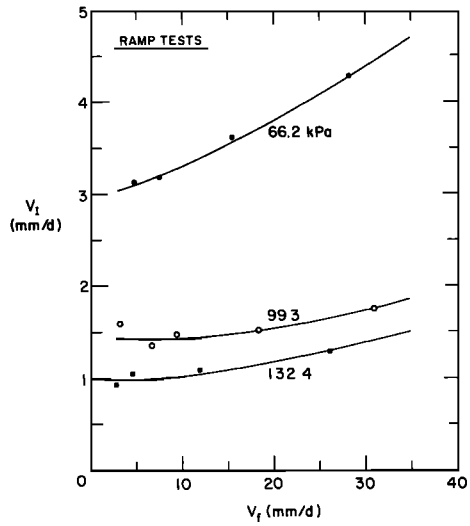

Fig. 16. Computed results for the same cases as in Figure 14 showing more rapid rise in heave rate versus freezing rate for lower overburdens.

boundary during heave. While the total ice body may be very complex in its microscopic geometry, it should move as a rigid body, with spatially uniform velocity. As it migrates, the pore ice accommodates the immobile soil matrix by melting where necessary on the warm sides of soil grains and refreezing on the cold sides. Thus in conjunction with the rigid ice assumption, regelation is assumed to be of fundamental importance in fitting together other contributing mechanisms. We find it difficult to conceive of plausible explanations, without rigid ice and regelation, which permit the observed growth of ice lenses within the frozen soil. A brief investigation of alternative assumptions finds them implausible. Nevertheless, in the absence of strict proof it must be acknowledged that this feature of the model still remains an assumption, however physically well motivated.

It is gratifying to see results emerge from the simulations which are reasonable with respect to laboratory experience. For example, in the lab scale step freeze cases simulated we see suppression of heave and increased ice penetration with greater overburden and also water expulsion with ultimate flow reversal in higher overburden cases. The model predicts the rhythmic formation of lenses in a recognized pattern: veritably microscopic, closely spaced lenses during early rapid freezing, with larger lenses and lens spacings during later, slower freezing. We also see an increase in the ice segregation ratio associated with a decline in freezing rate, other things being equal. In cases with ramped boundary temperatures, producing steadier freezing and heave rates, simulated results feature shapes, influences, and trends which also characterize lab results in comparable cases. Simulations over much longer times and larger spaces take into account the effects of varying overburden on the heaving zone, showing a peak in the ice segregation ratio achieved. This makes sense in terms of our experience on the lab scale.

Alongside these positive points we note a number of challenges which remain. As it now stands, the model requires a great deal of computational effort under many circumstances, because the inception and growth of each individual lens must be simulated. It may be possible to bypass much of this by judiciously computing only representative portions of each stratum. Also, it is possible that one might obtain results similar to those produced by this complex model using a simpler version containing its presumably essential features. Work along the latter lines is being currently pursued.

A substantial challenge presented by the model is that of parameter identification. In the simulations reported here, we have used reasonable estimates and generalizations from quite limited data. Development of adequate data to characterize such sensitive parameters as unfrozen water content and hydraulic conductivity of the frozen fringe is not only time consuming and expensive; it also challenges the limits of our laboratory techniques. Eventually, it may be possible to use information from detailed validation of the model to reduce the number of independent quantities considered, to dismiss some as less important, and to employ a stochastic treatment of others. However, this can only follow strict verification of the basic structure of the model, which, in turn, requires experimental work of higher resolution than what has been done to date.

Lastly, we note that the approach propounded here provides a sufficient set of equations to obtain solutions for all obviously crucial quantities. However, this still allows the possibility that we have failed to quantify important additional interactions. In particular, our conceptualization of the rigid ice regelation system in the frozen fringe requires an active microscopic recirculation of water and heat around the soil grains. Yet no specific characterization of those processes appears explicitly in the macroscopic equations and parameters ultimately brought to bear. It may become apparent that additional mechanics and thermodynamics must be drawn upon to include adequately at the macroscopic level the roles and the limiting factors for the transport of adsorbed film water and the pore constituents. In any case, generalization of the theory to cover three (liquid water, ice, air) phases is necessary before the unsaturated case can be attacked. Important beginnings have already been made in this domain [e.g., *Miller*, 1973; *Colbeck*, 1982]. In addition, any application of our concepts to multidimensional situations will require substantially more sophisticated soil mechanics than is included here.

The forces of nature acting on engineering projects in northern regions increasingly motivate interest in the challenge of frost heave analysis. The results presented here motivate us to use this model as a starting point for addressing the substantial challenges which remain.

Acknowledgments. This work was supported in part by the Office of the Federal Inspector, Alaska Natural Gas Transportation System, and in part by National Science Foundation grants ENG-77-17004 and CEE-8017422. One of us (K.O.) was also supported in part by joint funding from the Federal Highway Administration, the U.S. Army Corps of Engineers, and the Federal Aviation Administration, under Intra-Governmental Order 5-3-0202. At the same time, this publication does not imply endorsement by any of those sponsors. The authors also gratefully acknowledge the benefit of helpful criticisms and numerous suggestions offered by reviewers of the original manuscript.

REFERENCES

Aitchison, G. D., Relationships of moisture stress and effective stress in unsaturated soils, in *Pore Pressure and Suction in Soils*, pp. 47–52, Butterworths, London, 1961.

Bresler, E., D. Russo, and R. D. Miller, Rapid estimate of unsaturated hydraulic conductivity function, *Soil Sci. Soc. Am. J.*, *42*, 170–172, 1978.

Chamberlain, E., Frost susceptibility of soil, Review of index tests, *CRREL Monogr. 81-2*, Cold Reg. Res. and Eng. Lab., Hanover, N. H., 1981.

Colbeck, S. C., Configuration of ice in frozen media, *Soil Sci., 133*, 116–123, 1982.

deVries, D. A., Thermal properties of soils, in *Physics of the Plant Environment*, edited by W. R. vanWijk, North-Holland, Amsterdam, 1963.

Fuchs, M., G. S. Campbell, and R. I. Papendick, An analysis of sensible and latent heat flow in a partially frozen unsaturated soil, *Soil. Sci. Soc. Am. J., 42*, 379–385, 1978.

Gilpin, R. R., A model for the prediction of ice lensing and frost heave in soils, *Water Resour. Res., 16*, 918–930, 1980.

Hoekstra, P., Water movement and freezing pressures, *Soil Sci. Soc. Am. J., 33*, 512–518, 1969.

Hoekstra, P., and R. D. Miller, Movement of water in a film between glass and ice, *CRREL Rep. 153*, Cold Reg. Res. and Eng. Lab., Hanover, N. H., 1965.

Hopke, S., A model for frost heave including overburden, *Cold Reg. Sci. Technol., 3*, 111–127, 1980.

Horiguchi, K., and R. D. Miller, Experimental studies with frozen soil in an ice sandwich permeameter, *Cold Reg. Sci. Tech., 3*, 177–183, 1980.

Horiguchi, K., and R. D. Miller, Hydraulic conductivity functions of frozen materials, in *Permafrost: Fourth International Conference*, National Academy Press, Washington, D. C., 1983.

Johansen, O., Thermal conductivity of soils, *Draft Transl. 637*, U.S. Army Cold Reg. Res. and Eng. Lab., Hanover, N. H., 1977.

Koopmans, R. W. R., and R. D. Miller, Soil freezing and soil water characteristic curves, *Soil Sci. Soc. Am. J., 30*, 680–685, 1966.

Loch, J. P. G., and B. D. Kay, Water redistribution in partially frozen, unsaturated soil under several temperature gradients and overburden loads, *Soil Sci. Soc. Am. J., 42*, 400–406, 1978.

Mellor, M., and R. Testa, Effect of temperature on the creep of ice, *J. Glaciol., 8*, 131–145, 1969.

Miller, R. D., Soil freezing in relation to pore water pressure and temperature, paper presented at 2nd International Conference on Permafrost, Natl. Acad. Sci., Yakutsk, USSR, 1973.

Miller, R. D., Frost heaving in non-colloidal soils, in *Proceedings, 3rd International Conference on Permafrost*, National Research Council of Canada, Edmonton, Alberta, 1978.

Miller, R. D., Freezing phenomena in soils, in *Applications of Soil Physics*, Academic, 1980.

Miller, R. D., and E. E. Koslow, Computation of rate of heave versus load under quasi-steady state, *Cold Reg. Sci. Technol., 3*, 243–252, 1980.

O'Neill, K., The physics of mathematical frost heave models: A review, *Cold Reg. Sci. Technol., 6*, 275–291, 1983.

O'Neill, K., and R. D. Miller, Numerical solutions for a rigid-ice model of secondary frost heave, *CRREL Rep. 82-13*, Cold Reg. Res. and Eng. Lab., Hanover, N. H., 1982.

Penner, E., Thermal conductivity of frozen soils, *Can. J. Earth Sci., 7*, 982–987, 1970.

Penner, E., and T. Ueda, The dependence of frost heaving on load application, *Intl. Symp. Frost Action Soils, Lulea, Sweden, 1*, 92–101, 1977.

Pinder, G. F., and W. G. Gray, *Finite Element Simulation in Surface and Subsurface Hydrology*, Academic, New York, 1977.

Römkens, M. J. M., and R. D. Miller, Migration of mineral particles in ice with a temperature gradient, *J. Colloid Interface Sci., 42*, 103–111, 1973.

Snyder, V. A., Theoretical aspects and measurement of tensile strength in unsaturated soils, Ph.D. thesis, Cornell Univ., 1980.

Snyder, V. A., and R. D. Miller, Tensile strength of unsaturated soils, *Soil Sci. Soc. Am. J.*, in press, 1985.

Tice, A. R., C. M. Burrous, and D. M. Anderson, Determination of unfrozen water in frozen soil by pulsed nuclear magnetic resonance, *Proceedings, 3rd International Conference on Permafrost*, pp. 149–155, National Research Council of Canada, Edmonton, Alberta, 1978.

R. D. Miller and K. O'Neill, Cold Regions Research and Engineering Laboratory, Hanover, NH 03755.

(Received November 29, 1983;
revised November 1, 1984;
accepted November 15, 1984.)